Power Electronics and Drives
Volume 10(45), 2025 DOI: 10.2478/pead-2025-0028

ANN Optimised RPWM Technique for Minimisation of Conducted EMI in Three-Phase Voltage Source Inverters

Research paper

Abdul Mumin Halidu[1,2,*], Solomon Nunoo[1], Joseph Cudjoe Attachie[1]

[1]*Department of Electrical and Electronic Engineering, University of Mines and Technology, Tarkwa, Ghana*
[2]*Department of Electrical and Electronic Engineering, Dr. Hilla Limann Technical University, Wa, Ghana*

Received: 10 September 2025; Received in the revised form: 10 November 2025; Accepted: 13 November 2025

Abstract: Sinusoidal pulse width modulation (SPWM) is a conventional control technique for three-phase voltage source inverters (VSIs), but it often introduces electromagnetic interference (EMI) and acoustic noise in connected induction loads. Random pulse width modulation (RPWM) offers better EMI performance but suffers from inefficient DC bus utilisation and residual harmonic clusters. This study proposes an artificial neural network (ANN)-optimised RPWM technique to more effectively disperse harmonic energy across a wider frequency spectrum. The ANN-generated modulation signal was integrated into a three-phase VSI with a passive L(Inductor), C(Capacitor) (LC) filter and evaluated against dual random and fixed PWM strategies in MATLAB/Simulink (Mathworks MATLAB R2023a) using power spectral density (PSD) and total harmonic distortion (THD) analyses. Results show that the ANN-based RPWM reduces conducted EMI and achieves a THD of 2.17%, with only a negligible increase in computational cost and no additional hardware requirements, offering a practical and cost-efficient approach for EMI reduction in inverter systems.

Keywords: *pulse width modulation • artificial neural network • harmonics • inverter • waveform*

1. Introduction

The widespread use of power converters has fuelled growing interest in the field of power electronics. At the core of this discipline are semiconductor devices, which play a crucial role in switch design, enabling the high-speed commutation required by power converters. These switching operations produce signals characterised by high rates of voltage and current change (dv/dt and di/dt), leading to broadband perturbations (Mahalik and Kos, 2005). Since power electronic devices are typically interconnected via power supply lines, these wide-band signals propagate along the lines and contribute to electromagnetic pollution, a phenomenon referred to as conducted electromagnetic interference (EMI) (Kazem, 2007; Kuebrich et al., 2005).

Pulse width modulation (PWM) remains the most widely adopted control strategy for voltage source inverters (VSIs) (Haq Syed Abdul et al., 2021), offering precise control of the fundamental output frequency and attenuation of certain harmonic components (Madasamy et al., 2021). Nonetheless, significant harmonics with notable amplitudes persist across much of the output voltage spectrum. Some researchers have resulted to increasing the inverter switching frequency to address this (Kaboli et al., 2007; Madasamy et al., 2021) or employing inverter topologies with additional switches (Makhubele and Ogudo, 2021; Muthukumar and Mary, 2014).

Alternatively, random pulse width modulation (RPWM) techniques aim to distribute harmonic energy over a wider frequency range, thereby reducing concentrated harmonic peaks (Wang et al., 2003). However, due to insufficient randomness in switching frequencies, RPWM methods often struggle to maintain high DC-link voltage

* *Email: amhalidu@dhltu.edu.gh*

levels (Madasamy et al., 2021). This limitation results in residual harmonic content even at elevated switching frequencies and can potentially excite system resonances (Peyghambari et al., 2016).

Recent developments in machine learning have opened new avenues in power electronics, offering notable benefits (Mathews et al., 2022). This has motivated an in-depth investigation into the application of machine learning, specifically artificial neural network (ANN), to enhance RPWM performance by increasing switching randomness and reducing both harmonic content and residual clusters in converter output waveforms. This study explores the use of ANNs to overcome the limitations of conventional RPWM, aiming to further reduce the total harmonic distortion (THD) in the output voltage of a three-phase VSI.

An ANN-generated signal is integrated into a modified RPWM scheme, combined with three sinusoidal reference signals and a dual-random triangular carrier signal to form the switching pulse. A first-order passive LC low-pass filter is also employed to improve waveform quality. This approach minimises the number of inverter switches, thereby reducing switching losses and emphasises technique optimisation rather than hardware addition, resulting in lower costs and improved efficiency. As such, the proposed system does not incur any significant hardware cost increase, with only a negligible computational overhead (≈1%) associated with ANN inference. The method, therefore, offers a cost-effective, software-based enhancement to existing RPWM strategies while improving efficiency and EMI performance. The goal is to achieve a broader dispersion of harmonic clusters and reduce acoustic noise levels in RPWM-controlled VSIs. To validate the effectiveness of the proposed system, it is compared against a dual random pulse width modulated (DRPWM) three-phase VSI and a conventional fixed carrier signal modulated (FCSM) VSI, which is akin to sinusoidal pulse width modulation (SPWM). Power spectral density (PSD) analysis is performed using Welch's method in MATLAB/Simulink, while fast fourier transform (FFT) analysis is used to evaluate THD levels. Results demonstrate that the proposed method achieves a more uniform harmonic spread over a wider frequency range compared to both DRPWM and SPWM approaches.

2. Framework

2.1. Modulating principle of the RPWM

To reduce acoustic noise in motor drives, various researchers have explored techniques involving randomisation of the switching frequency. Madasamy et al. (2021) introduced randomness by varying the switching frequency through space vector modulation (SVM) using an asymmetric frequency multicarrier. Kirlin et al. (2011) implemented randomised inverter switching around a nominal frequency, while Bech et al. (2000) randomised the switching frequency by altering the distribution of the zero vector within each switching cycle. These methods introduce non-deterministic elements into the output waveform (Lai et al., 2013; Liaw et al., 2000), which effectively convert narrow-band acoustic noise into broad-band noise by dispersing the harmonic spectrum away from the switching frequency (Binojkumar et al., 2013; Mathe et al., 2012). However, this approach tends to increase waveform distortion due to the randomness, and the average inverter switching losses remain comparable to those of deterministic PWM strategies (Mathe et al., 2012).

Further studies have focussed on applying RPWM techniques using the SVM method. (de Oliveira et al., 2005; Khan et al., 2010; Lee et al., 2000) randomly sampled the reference voltage space vector and achieved averaging by switching among its three nearest vectors. In other studies, including George and Baiju, (2013) and Madasamy et al. (2021), the switching frequency was varied randomly within predefined bounds, producing randomly spaced samples without requiring sector identification. George and Baiju (2013) further noted that the reference phasor is mapped into a vector within a two-level inverter, enabling calculation of switching time vectors. These strategies have demonstrated significant reductions in both acoustic noise and EMI. However, as Makhubele and Ogudo (2020) highlighted, such methods are often complex, computationally demanding and expensive to implement.

Owusu et al. (2023) employed ANNs to optimise a sinusoidal PWM-based controller for a three-phase VSI, achieving promising results. Nonetheless, the deterministic nature of the output results in harmonic clustering around the switching frequency, which contributes to increased noise in motor drives.

The modulation principle underlying the RPWM technique has been extensively examined by several researchers (Jadeja et al., 2015; Kim et al., 2004; Lee et al., 2016). In its implementation, three reference signals S_a, S_b and S_c are individually compared with a single randomised triangular carrier signal C, to generate the switching pulses for each leg of the three-phase VSI. Figure 1 illustrates the modulation principle of the RPWM technique.

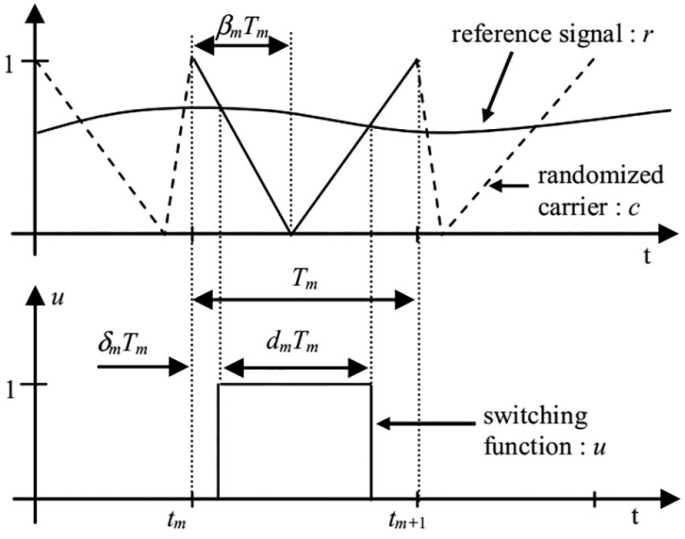

Figure 1. Modulating principle of RPWM. RPWM, random pulse width modulation.

In this context, the switching function *u*, for each phase of the inverter, is determined by the switching period (*T*), the delay factor (δ), and the duty cycle (*d*). In practical implementations, the reference signals are deterministic (uniform and phase-shifted by 2π/3), allowing for effective control of the output voltage. Consequently, only the switching period and delay factor are subject to randomisation. This is achieved using a triangular carrier signal defined by its period *T* and a fall-time delay β.

The randomisation of these parameters is facilitated by a linear congruential generator (LCG), which uses a uniform probability distribution and applies statistical averaging techniques, as described in the studies of Bhattacharya et al. (2015), Boudjerda et al. (2011), and Boudouda et al. (2012).

The random variation of *T* is implemented between the interval [T_{min}, T_{max}], by using the statistical mean

$$\overline{T} = \frac{1}{Fs} \tag{1}$$

where *Fs* = switching frequency = 3,000 Hz; the randomness level

$$R_T = \left[\frac{T_{\max} - T_{\min}}{\overline{T}}\right] \tag{2}$$

$$\text{then, } \rightarrow T \in \left[\overline{T}\left(1 - \frac{rt}{2}\right), \overline{T}\left(1 + \frac{rt}{2}\right)\right]$$

The random variation of the parameter β is implemented within the interval

$$\left[\beta_{min},\ \beta_{max}\right] \text{ with } \beta_{min} \geq 0 \text{ and } \beta_{max} \leq 1, \text{ the statistical mean } \overline{\beta} = 0.5,$$

and the randomness level is calculated as

$$R_\beta = \left[\frac{\beta_{\max} - \beta_{\min}}{\overline{\beta}}\right] \tag{3}$$

with $0 \leq R_\beta \geq 2$; then therefore,

$$\beta \in \left[\overline{\beta}\left(1 - \frac{R_\beta}{2}\right),\ \overline{\beta}\left(1 + \frac{R_\beta}{2}\right)\right]$$

When the parameters *T* and β are held constant in triangular signal generation, the result is a triangular waveform with fixed characteristics. When this fixed waveform is compared with sinusoidal reference signals, the modulation technique is classified as deterministic or classical SPWM.

Randomising the parameter *T* results in random carrier frequency *M* = modulation (RCFM), while randomising β leads to random pulse positioning modulation (RPPM), both in reference to the sinusoidal signals.

When both *T* and β are randomised simultaneously, the approach is termed dual random pulse width modulation (DRPWM). Compared to RCFM and RPPM individually, DRPWM exhibits superior spectral spreading capabilities, as demonstrated in the studies by Boudjerda et al. (2011) and Boudouda et al. (2012). In this study, a dual-randomised carrier signal *c*(*t*) is generated using a MATLAB Function block, with time (*t*), switching period *T* and fall-time delay β as inputs. This synthesised signal serves as a core component of the dataset used to train the ANN.

2.2. ANN signal generation

An ANN was developed using a supervised feedforward architecture with backpropagation, trained with known target outputs (Ali and Mashwani, 2023). It comprised 3 layers: an input layer with 4 neurons, a hidden layer with 10 neurons and an output layer with 3 neurons. Inputs combined three sinusoidal reference signals and a random signal from a MATLAB Function block. After training, the network generated three control signals, later combined with reference and triangular carrier signals for modulation.

Figure 2 illustrates the network's structure, showing connections between layers via weights ('M') and biases ('B'). Weights, initialised randomly between 0 and 1, adjust input signals through the network, while biases shift the activation function's input. Each hidden layer neuron computes a weighted sum of its inputs, followed by a sigmoid activation function to model non-linear relationships expressed as;

$$W = \left(R_1 \times M_1\right) + \left(R_2 \times M_{11}\right) + \left(R_3 \times M_{21}\right) + \left(C \times M_{31}\right) + B_1 \tag{4}$$

The network was trained using the 'trainlm' function, which implements the Levenberg-Marquardt Optimisation (LMO) algorithm. This method was selected for its robustness, efficiency and high accuracy with smaller datasets. LMO is well-suited for moderate-sized feedforward networks, balancing the speed of Gauss-Newton with the stability of gradient descent. During optimisation, the Hessian matrix H is approximated using the Jacobian J.

$$X_{K+1} = X_K - [J^T + \mu I]^{(-1)} J^T e \tag{5}$$

The scalar value μ was initially set to 0 to allow the Hessian matrix approximation in Newton's method. During optimisation, μ was adjusted to control the step size, decreasing μ enabled larger steps and improving the reduction of the performance function. This function was estimated using the Hessian $H = J^T J$, while the gradient was computed as follows:

$$g = J^T e \tag{6}$$

With J representing the Jacobian matrices and *e* as the error.

The mean squared error (MSE) method was employed during the training process to evaluate the performance of the network, mathematically expressed as:

$$MSE = \frac{\sum \left(y - \hat{y}_i\right)^2}{n} \tag{7}$$

where n is the number of observations, y is the i^{th} observed value and $\hat{y}_i$ is the corresponding predicted value

The back propagation (BP) learning algorithm was utilised to update the network's weights and minimise the MSE. The weight update process in BP is mathematically represented as:

$$W\left(i+1\right) = w\left(i\right) - \eta g\left(i\right) \tag{8}$$

where η represents the learning rate and $g(i)$ represents the gradient vector

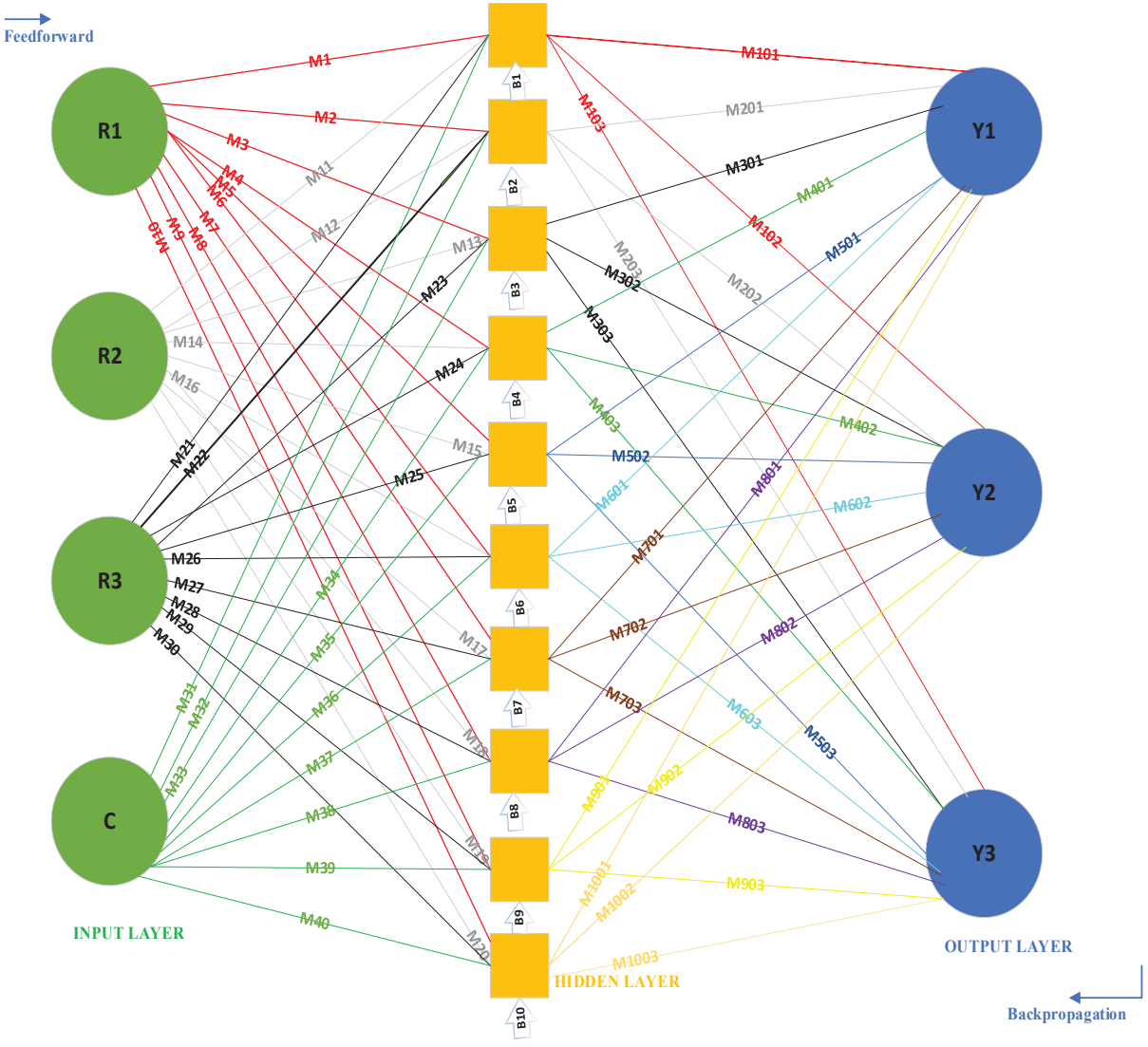

Figure 2. ANN architecture. ANN, artificial neural network.

During backpropagation, the chain rule was used to compute the gradient vector. For training, dual random carrier signals combined with three sinusoidal reference signals comprised 70% of the dataset, with the remaining 30% reserved for validation. Both *feedforwardnet* and *cascadeforwardnet* were tested, showing similar performance. These functions can approximate any finite input-output mapping with sufficient hidden neurons, using a 1 × N vector of hidden layer sizes and the *trainlm* backpropagation algorithm. The input and output layer sizes are initially set to zero and adjusted automatically during training. The *feedforwardnet* was ultimately chosen for its simplicity and fast convergence in solving fitting problems. Table 1 summarises the training data, while Figures 3 and 4 display the training results.

The proposed ANN modifies the random carrier index to minimise both harmonic distortion and conducted EMI. The ANN receives three normalised inputs: modulation index m_a, reference voltage amplitude V_{ref} and instantaneous current i_o. The output neuron produces an adaptive carrier frequency shift factor Δfc, governing the instantaneous carrier frequency $fc(t) = f_{base} + \Delta fc$. The network is trained using the Levenberg–Marquardt (LM) algorithm to minimise

$J = \alpha THD + \beta P_{EMI}$; where α and β weigh the trade-off between waveform quality and spectral spread. The LM algorithm iteratively updates weight matrices W and biases b as $W_{k+1} = W_k - \left(J_k^T J_k + \mu I\right)^{-1} J_k^T e_k$ ensuring rapid convergence with low computational overhead. The trained ANN is implemented in the MATLAB/Simulink model

Table 1. ANN training parameters.

Parameters	Values
Network type	Feedforward/backpropagation
Learning algorithm	Trainlm
Epochs	1,000
Convergence limit (Goal)	$1e^{-12}$
Hidden layers	10
Input layers	4
Output layers	3

ANN, artificial neural network.

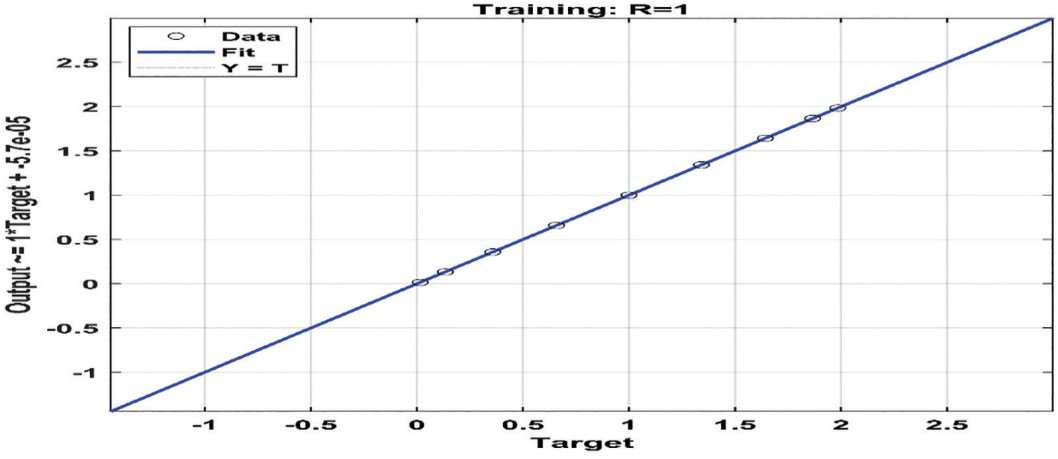

Figure 3. Output regression line after training.

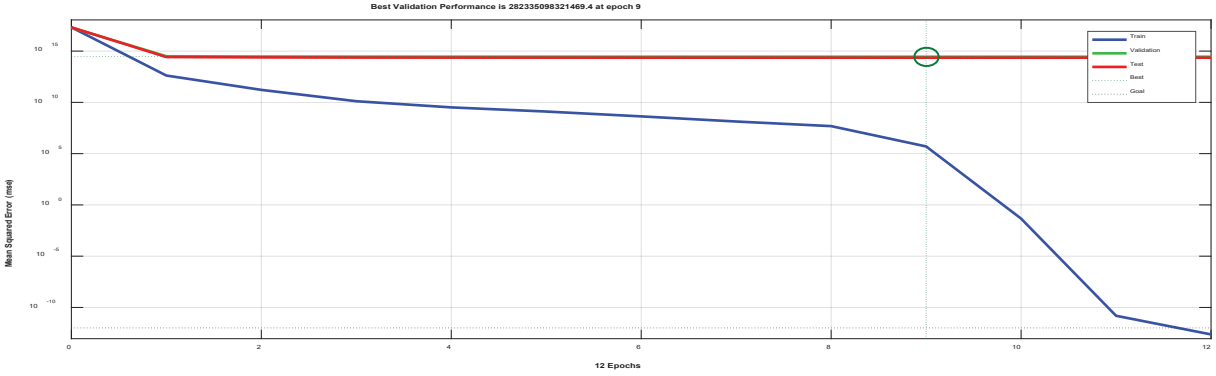

Figure 4. MSE output curve after training. MSE, mean squared error.

through a feed-forward structure requiring approximately 2×10^4 FLOPs per cycle, easily manageable by mid-range DSPs such as TI TMS320F28379D.

2.3. Implementation of the proposed method

The proposed method improves the RPWM strategy, which is preferred over conventional PWM for controlling three-phase VSIs due to its ability to spread harmonic clusters across a wider frequency range (Addo-Yeboah and Owusu, 2022; Sohaib Sajid et al., 2020). RPWM typically combines a sinusoidal reference with a randomly varied carrier to generate switching pulses (Raju et al., 2013). In this approach, an ANN-generated signal is added to the reference and carrier signals to enhance pulse generation. A low-pass LC filter further smooths the output, reducing THD and improving waveform quality, efficiency and overall performance.

2.4. Pulse generation signals

A randomly varied triangular signal *C*(*t*) is generated by setting two parameters: the period *T* and the fall-delay time β. The waveform's first and second halves are defined by Eqs (9)–(16).

For the fixed triangular carrier in FCSM, Eqs (9)–(12) are applied:

$$T = Ts \tag{9}$$

$$B = \frac{T}{2} \tag{10}$$

$$T = T + Ts \tag{11}$$

$$B = \frac{T + Ts}{2} \tag{12}$$

Whereas for the random triangular carrier in the DRPWM, Eqs (13)–(16) are applied

$$T = T_{\min} + (rand \times (T_{\max} - T_{\min})) \tag{13}$$

$$\beta = T_0 \times (b_{\min} + (rand \times (b_{\max} - b_{\min}))) \tag{14}$$

$$T = T_0 \times (b_{\min} + (rand \times (b_{\max} - b_{\min}))) \tag{15}$$

$$\beta = T_2 \times (b_{\min} + (rand \times (b_{\max} - b_{\min}))) \tag{16}$$

where:

$$T_{\max} = T_s \times \left(1 + \frac{rt}{2}\right) \tag{17}$$

$$T_{\min} = T_s \times \left(1 - \frac{rt}{2}\right) \tag{18}$$

where $T_{\max}$ is the random upper period limit and $T_{\min}$ is the random lower period limit, for $rt = 0.2$ where rt is the period randomness level. Also,

$$b_{\max} = 0.5 \times \left(1 + \frac{rt}{2}\right) \tag{19}$$

$$b_{\min} = 0.5 \times \left(1 - \frac{rt}{2}\right) \tag{20}$$

where $b_{\max}$ is the random upper amplitude limit and $b_{\min}$ is the random lower amplitude limit, for $rb = 2$ with rb, the amplitude randomness level.

Eventually, *C(t)* was generated with *t* as the time input factor for the MATLAB function block and was used as the principal part of the input data of the ANN.

Three sinusoidal signals with a phase shift of 120° were generated for training purposes using the following Eqs (21)–(23)

$$R_1(t) = sin(100\pi t) \tag{21}$$

$$R_2(t) = sin\left(100\pi t + \frac{2\pi}{3}\right) \tag{22}$$

$$R_3(t) = sin\left(100\pi t - \frac{2\pi}{3}\right) \tag{23}$$

Subsequently, four signals served as the input signals in the ANN training.

$$Input\_Net = \left[R_1(t),\ R_2(t),\ R_3(t),\ C(t)\right] \tag{24}$$

Three target outputs, Y_1, Y_2 and Y_3, were obtained from the ANN supervised training using the four input signals for the proposed method, by applying the mathematical Eqs (25)–(27) for the proposed method.

$$Y_1(t) = \left[R_1(t) - C(t)\right] \tag{25}$$

$$Y_2(t) = \left[R_2(t) - C(t)\right] \tag{26}$$

$$Y_3(t) = \left[R_3(t) - C(t)\right] \tag{27}$$

3. Introduction of the Passive Filter

Passive filters, composed of inductors and capacitors, are used to attenuate high-frequency signals (Muhlethaler et al., 2013). To improve output waveform symmetry and reduce THD in the proposed method, a first-order low-pass filter was implemented. The DRPWM's initial spread-spectrum effect caused a steady roll-off, necessitating a lower frequency response. To balance performance and cost, several EMI filter topologies R(Resistor) C (Capacitor) (RC), R(Resistor) L(Inductor) (RL) and LC were evaluated. Among them, the LC low-pass filter offered effective attenuation with minimal trade-offs, such as side inductance, at a reasonable cost. As illustrated in Figure 5, the LC filter was designed and implemented based on Eqs (28) and (29) and compared against other passive and active filter configurations.

The values of *L* and *C* were calculated as below:

$$L = \frac{V_{dc}}{4 \times fs \times \Delta Ia} \tag{28}$$

$$C = \left(\frac{10}{2 \times \pi \times fs}\right)^2 \left(\frac{1}{L}\right) \tag{29}$$

where

V_{dc} = input voltage of inverter

%*Ia* = 20% of the load current

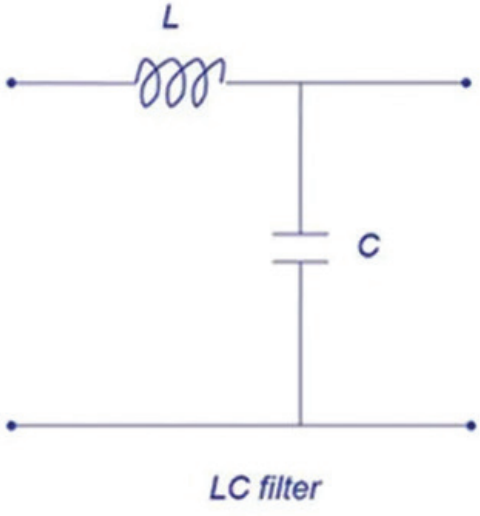

Figure 5. Single line diagram of LC low pass filter.

4. The Block Diagram of the Proposed Method

Figure 6 shows the combination of sinusoidal and random carrier signals used to generate ANN-based switching pulses for the three-phase inverter. An LC filter smooths the output before it is applied to a series R(Resistor) L(Inductor) C(Capacitor) (RLC) load. THD and PSD analysis were conducted, and the results are discussed in Section 6.

5. MATLAB Simulation of the Various Systems

This section presents simulations of three methods including FCSM (SPWM), DRPWM and the proposed approach under two conditions: before and after LC filtering in a three-phase VSI. As shown in Figure 7, a MATLAB function block was used to generate fixed and dual random carrier signals based on Eqs (9)–(12) and (13)–(16). These were compared with three sinusoidal reference signals (*Sa*, *Sb* and *Sc*) to produce switching pulses for the inverter. The combined signals controlled switches 1 and 4, 3 and 6, as well as 5 and 2 for the inverter's first, second and third legs, respectively. Figures 8 and 10 show the switching pulses for the first leg using FCSM and DRPWM.

The design of the three-phase VSI with the LC filter connected is shown in Figure 11.

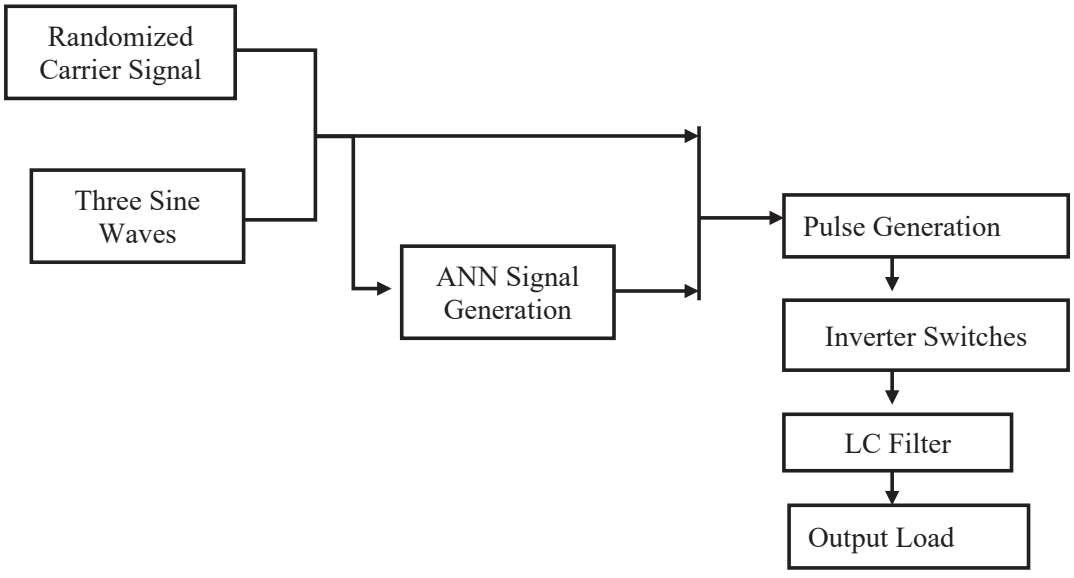

Figure 6. Block diagram of the proposed method. ANN, artificial neural network.

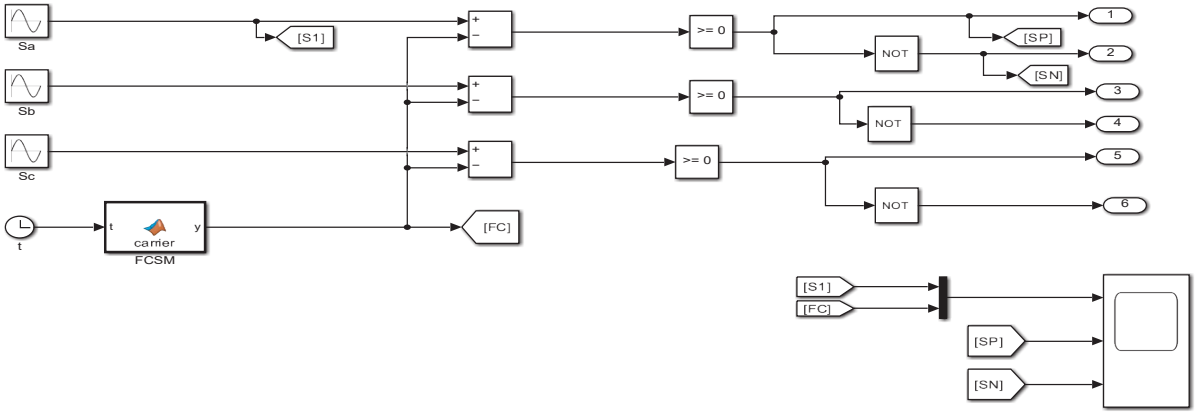

Figure 7. Switching pulse generation for FCSM. FCSM, fixed carrier signal modulated.

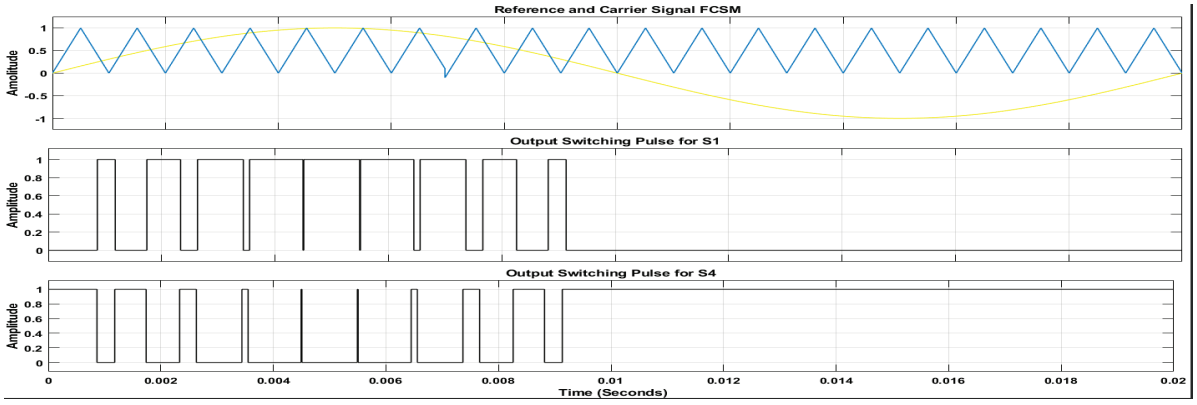

Figure 8. Pulse generation for the FCSM strategy on one leg of three phase inverter. FCSM, fixed carrier signal modulated.

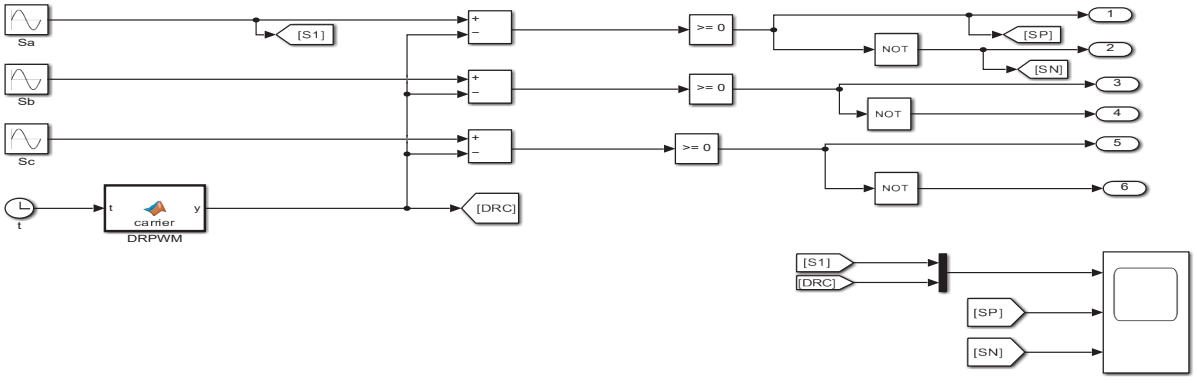

Figure 9. Switching pulse generation for DRPWM. DRPWM, dual random pulse width modulated.

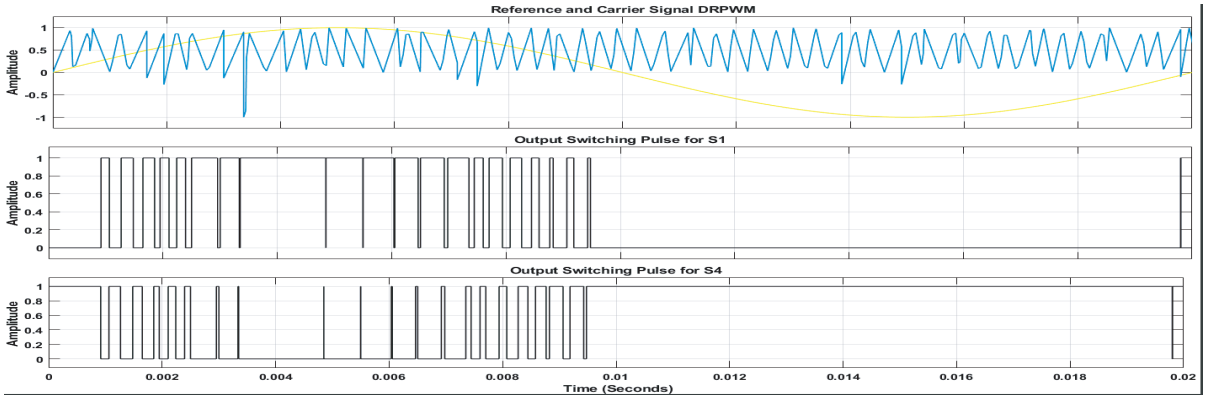

Figure 10. Pulse generation for the DRPWM strategy on one leg of three phase inverter. DRPWM, dual random pulse width modulated.

5.1. Simulation of the proposed method

The controller in Figure 12 was used to generate switching pulses for the proposed ANN-optimised method. The ANN was trained using the dual random carrier signal and three fundamental sinusoidal signals, as defined by Eqs (13)–(20). The resulting ANN signal was then combined with the sinusoidal and carrier signals to produce switching pulses for each leg of the three-phase VSI.

The control pulses generated for the switches in the first leg of the three-phase VSI are illustrated in Figure 13.

Figures 14–16 show the output voltage waveforms before and after LC filtering for the FCSM, DRPWM and proposed methods, respectively.

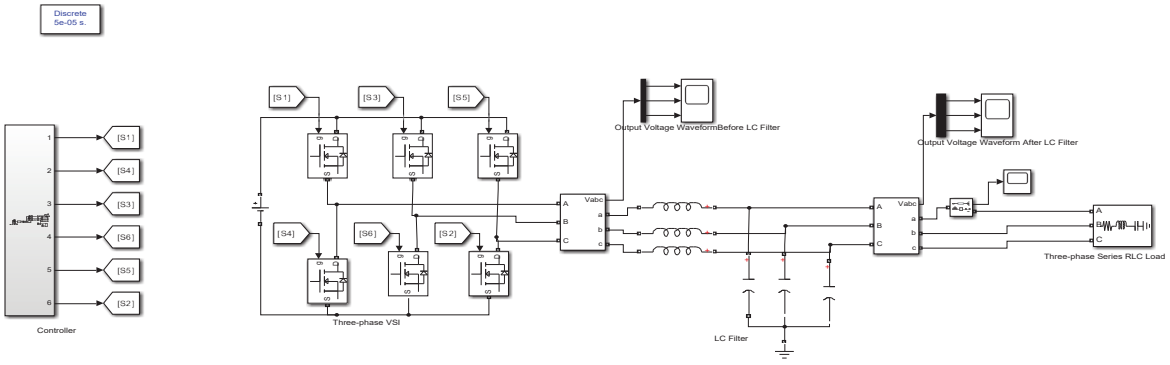

Figure 11. Diagram of the three-phase VSI. VSI, voltage source inverter.

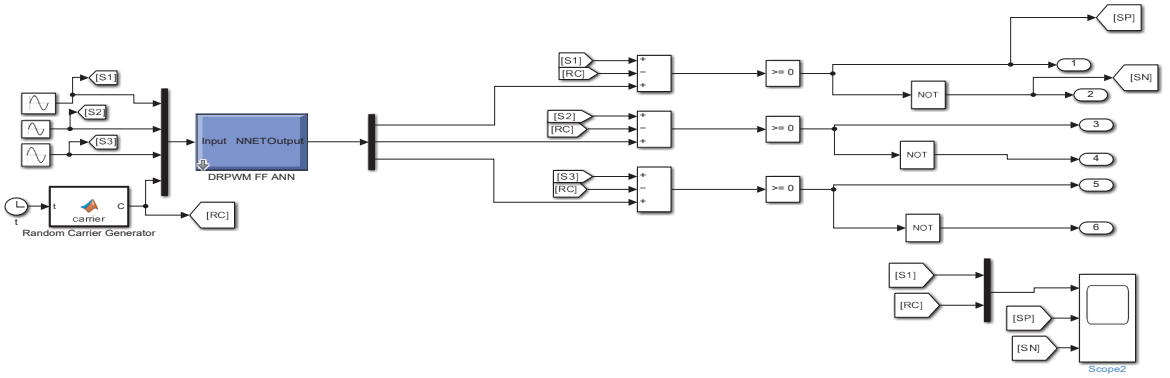

Figure 12. Pulse generation for ANN incorporated. ANN, artificial neural network.

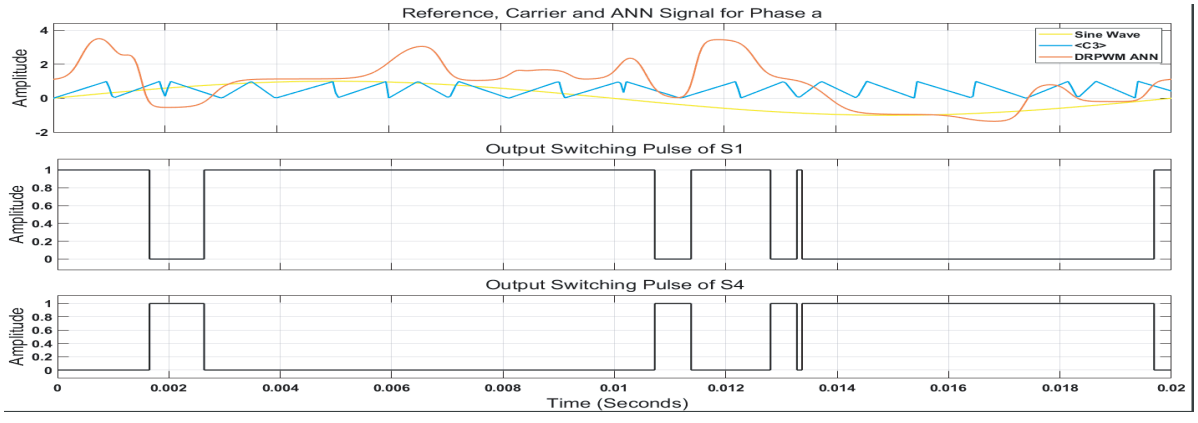

Figure 13. Pulse generation for the proposed strategy on one leg of three-phase inverter. ANN, artificial neural network; DRPWM, dual random pulse width modulated.

The output voltage waveforms, along with their THD and PSD analysis, are presented and discussed in the Section 6.

6. Results and Discussion

6.1. PSD analysis of the output voltage waveforms

PSD analysis was performed using Welch's method in MATLAB. Figures 17–19 show the PSD results for FCSM, DRPWM and the proposed ANN-optimised method, respectively.

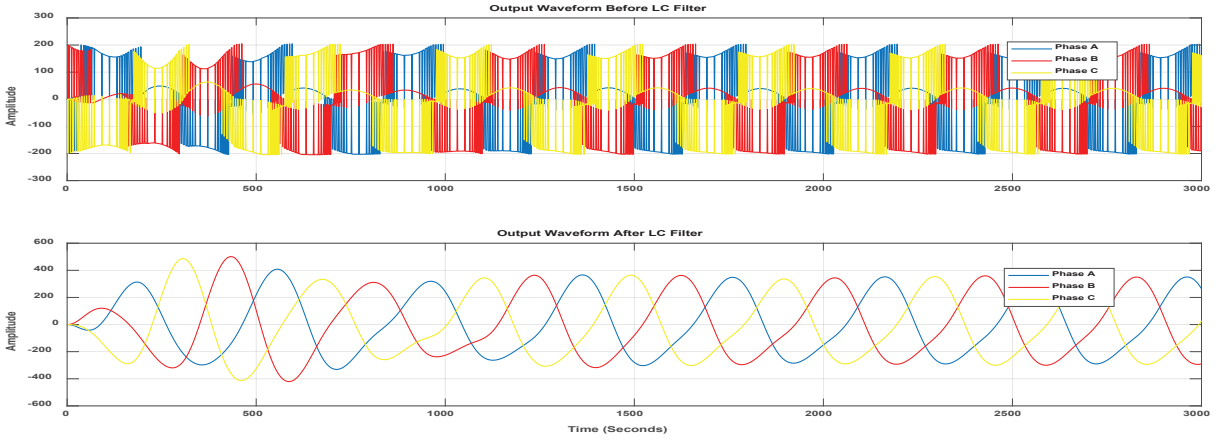

Figure 14. Output voltage waveform with and without an LC filter for FCSM. FCSM, fixed carrier signal modulated.

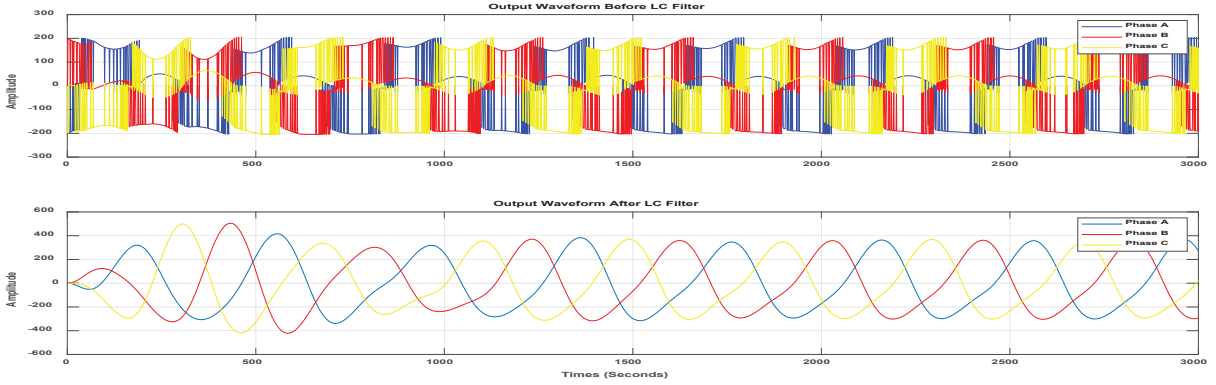

Figure 15. Output voltage waveform with and without LC filter for DRPWM. DRPWM, dual random pulse width modulated.

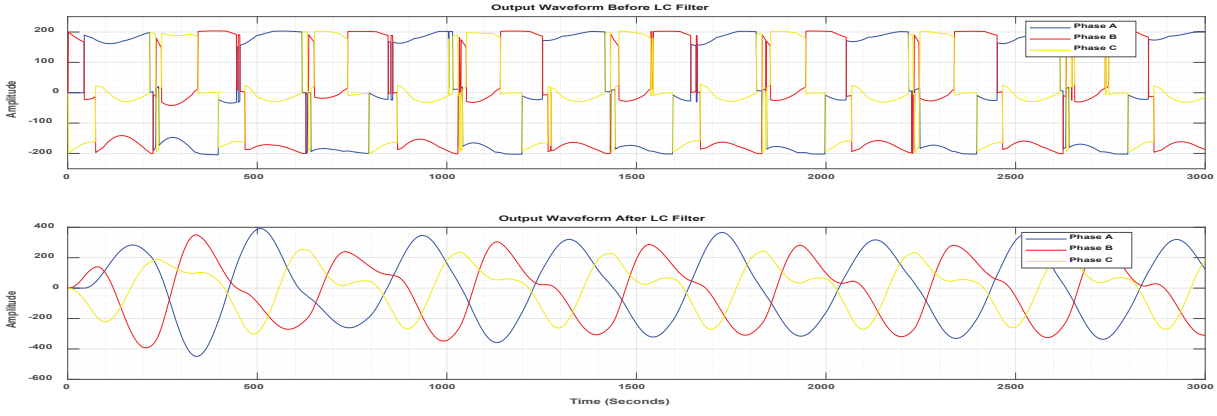

Figure 16. Output voltage waveforms before and after the LC filter for the proposed method.

6.2. THD analysis of the output voltage waveforms

The output voltage waveforms were analysed before and after the LC filter for all three methods. Controllers in Figures 7 and 8 implemented the FCSM and DRPWM methods on the three-phase VSI shown in Figure 11. The apparent amplitude rise is due to the filter's gain characteristics near its corner frequency, combined with the spectral redistribution introduced by random switching. The LC filter amplifies components near the cut-off frequency before full attenuation takes effect. Figures 20a, b show the FCSM method's THD levels before and after the LC filter, while Figures 21a, b show the same for the DRPWM method.

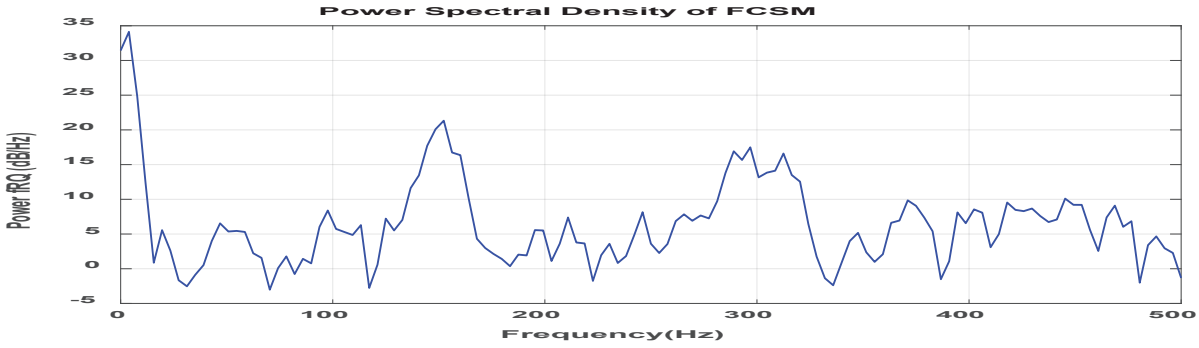

Figure 17. Output voltage PSD of FCSM. FCSM, fixed carrier signal modulated; PSD, power spectral density.

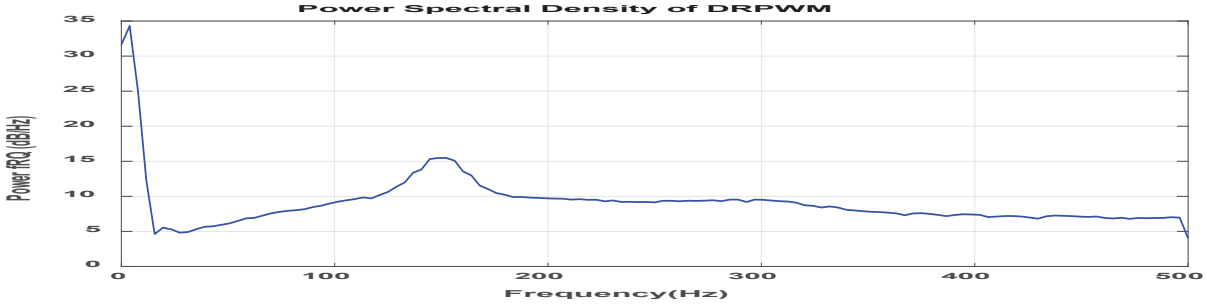

Figure 18. Output voltage PSD of DRPWM. DRPWM, dual random pulse width modulated; PSD, power spectral density.

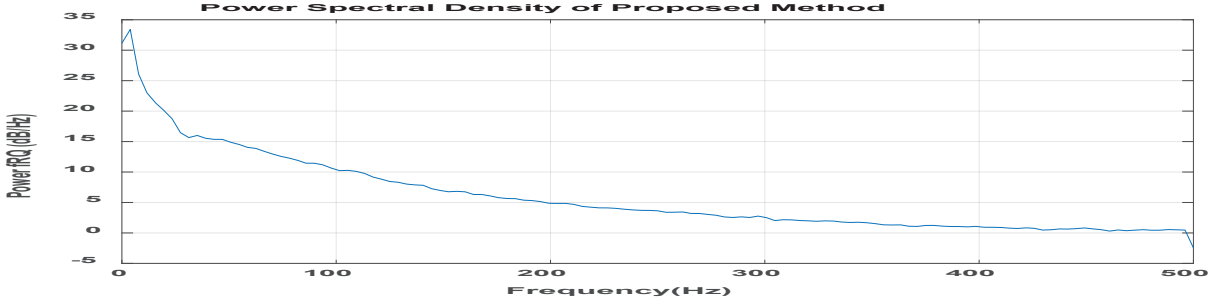

Figure 19. Output voltage PSD of the proposed method. PSD, power spectral density.

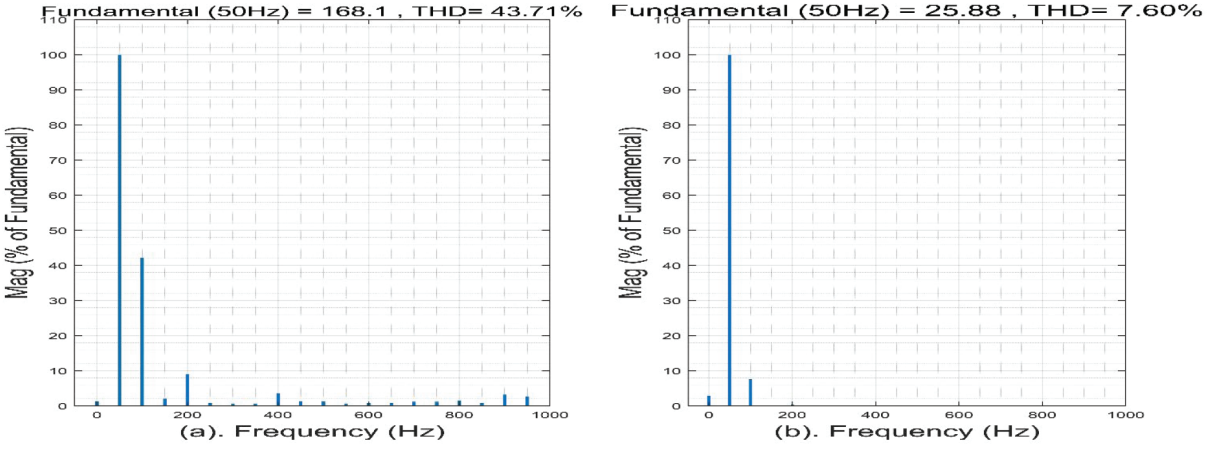

Figure 20. THD content of the FCSM. (a) Before and (b) after the LC filter. FCSM, fixed carrier signal modulated; THD, total harmonic distortion.

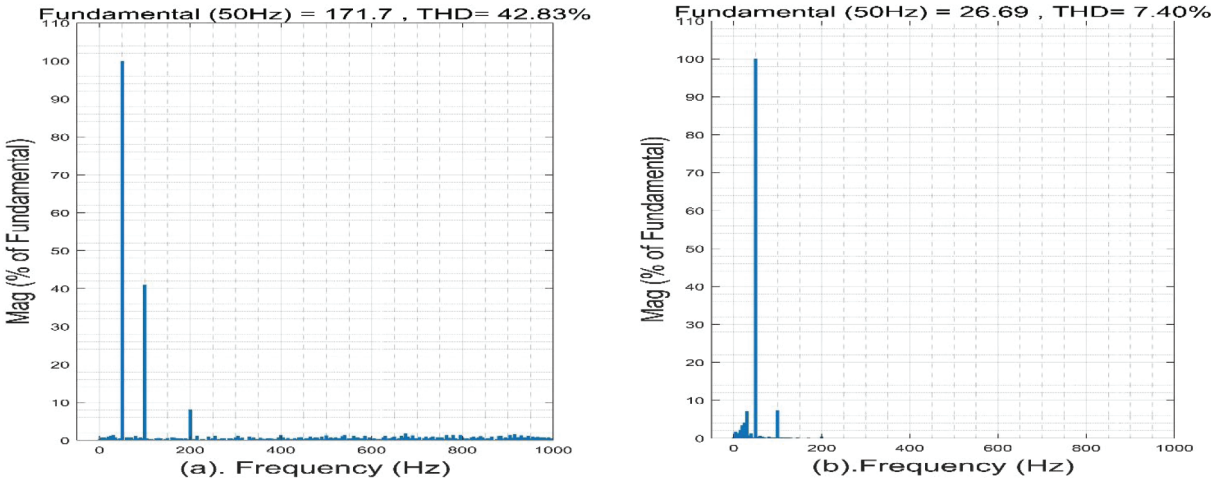

Figure 21. THD content of the DRPWM (a). Before and (b). After the LC filter. DRPWM, dual random pulse width modulated; THD, total harmonic distortion.

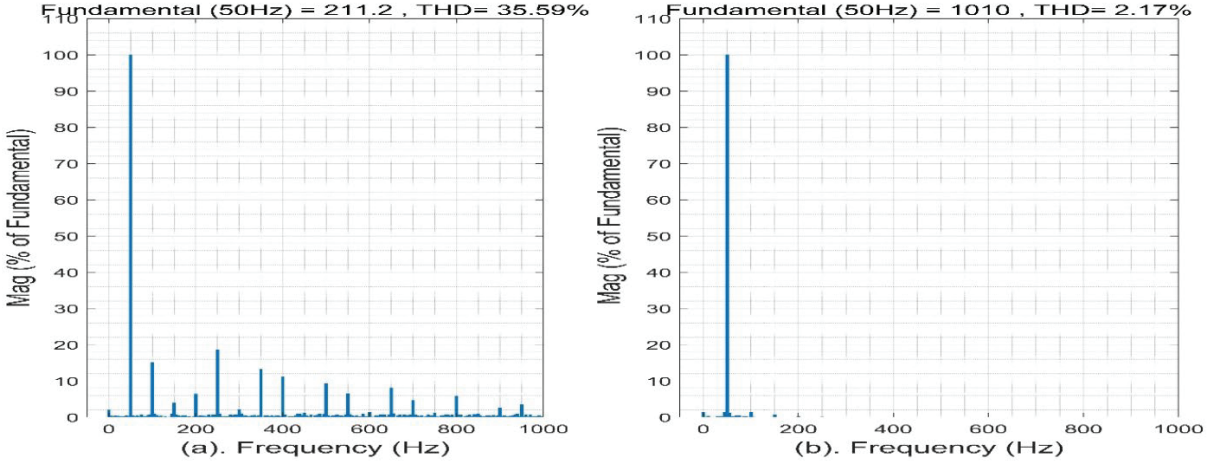

Figure 22. THD content of the proposed method. (a) Before and (b) After the LC filter. THD, total harmonic distortion.

The controller in Figure 12 was used to regulate the three-phase VSI (Figure 11), and the output voltage THD of the proposed method was evaluated before and after the LC filter, as shown in Figure 22.

Table 2 gives a summary of the THD content levels of the three simulations under the two conditions of before and after the LC filter connection.

6.3. Discussions on results

FFT-based harmonic analysis was conducted for the three modulation techniques. Table 3 lists the first six significant harmonics and their relative magnitudes, highlighting that the 5th and 7th harmonics are reduced by approximately 43% and 37%, respectively.

The results confirm that the ANN-RPWM achieves broader harmonic energy dispersion, yielding a flatter PSD and improved EMI attenuation.

6.3.1. Findings from the PSD analysis

The line-to-line output voltage PSD of the three modulation strategies shows a clear reduction in noise from FCSM to DRPWM. FCSM exhibits prominent peaks at the fundamental frequency and its harmonics, while DRPWM produces a more uniform PSD. ANN optimisation further improves noise attenuation, yielding lower peak levels and a flatter, more evenly distributed PSD.

Table 2. Summary of THD content levels (%).

System	THD before filter (%)	THD after LC filter (%)
FCSM	43.71	7.60
DRPWM	42.83	7.40
Proposed method	35.59	2.17

DRPWM, dual random pulse width modulated; FCSM, fixed carrier signal modulated; THD, total harmonic distortion.

Table 3. Summary of harmonics and their relative magnitudes.

Harmonic order	FCSM (dB)	DRPWM (dB)	ANN-RPWM (dB)	Reduction vs. DRPWM (%)
5	–36	–40	–46	43
7	–38	–42	–47	37
11	–40	–43	–48	35
13	–42	–44	–49	35

ANN-RPWM, artificial neural network-random pulse width modulation; DRPWM, dual random pulse width modulated; FCSM, fixed carrier signal modulated.

Table 4. Techno-economic comparison between conventional RPWM and proposed ANN-RPWM controller.

Cost component	Conventional RPWM system	Proposed ANN–RPWM system	Remarks/assumptions
DSP/microcontroller	Included	Same	No additional processor required
Power semiconductors (IGBTs/drivers)	6 IGBTs + 3 drivers	Same	Unchanged hardware configuration
Sensors/feedback circuits	3 V, 3 current sensors	Same	No modification needed
Software/algorithmic overhead	Baseline PWM control	+3% additional CPU load	ANN inference executed on the same DSP
Development/training effort	N/A	One-time offline training	Conducted using MATLAB on PC
Filter components (L, C)	LC filter	Same	Identical filter design used
Implementation/maintenance	Standard	Standard	No extra calibration required
Estimated total cost impact	100%	≈101%	<1% incremental difference

ANN-RPWM, artificial neural network-random pulse width modulation; DSP, digital signal processor; IGBT, Insulated Gate Bipolar Transistor; PC, Personal Computer; PWM, pulse width modulation; RPWM, random pulse width modulation.

6.3.2. Findings from the THD analysis

The output voltage from the optimised controller in Figure 11 effectively spreads the harmonic spectrum and reduces THD compared to both DRPWM (RPWM-based) and conventional FCSM (SPWM). THD was reduced from 42.83% to 35.59%, significantly lowering conducted emissions. With the LC filter, THD further decreased to 2.17%, meeting electromagnetic compatibility (EMC) standards. Table 2 summarises the THD levels achieved by the proposed method.

6.3.3. Projected cost and techno-economic evaluation

In addition to the projected component-based cost shown in Table 3, a concise techno-economic assessment was performed to evaluate the economic implications of the proposed ANN-optimised RPWM controller relative to a conventional RPWM inverter. The analysis considers hardware, software and computational overhead. The results are summarised in Table 4.

The data in Table 4 confirm that the ANN-RPWM strategy can be integrated into the same hardware platform as the conventional RPWM system without additional circuitry. The neural-network inference runs as a lightweight feed-forward operation on the existing controller, resulting in an estimated computational increase of only ≈ 3% and a total cost impact below 1%. This validates the claim in the abstract that the proposed method does not introduce a meaningful cost increase while improving harmonic suppression and EMI performance.

6.4. Practical implementation and experimental prospects

Although the study is simulation-based, the ANN-RPWM algorithm is readily deployable in real-time hardware. The feed-forward structure enables deterministic computation with an estimated execution time of ≈ 3 μs per switching cycle on a 200 MHz digital signal processor (DSP).

The controller requires no additional sensors or switching devices. Implementation can be realised using existing PWM modules with minor firmware modification. Future work will focus on hardware-in-loop testing using Software tool (dSPACE) and experimental validation on a 5 kVA three-phase VSI prototype driven by a Texas Instruments TMS320F28379D DSP will be used to reproduce the MATLAB/Simulink conditions equipped with a passive LC output filter and standard voltage and current sensing circuits. Conducted EMI and THD measurements will be performed using a line impedance stabilisation network (LISN) and a spectrum analyser in accordance with CISPR 16-1 standards. This hardware arrangement will enable direct comparison between simulated and experimental results, providing practical verification of the ANN-RPWM controller's effectiveness in reducing EMI and harmonic distortion.

7. Conclusion

This study presents a novel three-phase VSI controller that enhances harmonic spreading in RPWM by integrating an ANN trained via feedforward/backpropagation. The ANN generates an additional modulation signal combined with dual random triangular carriers to produce switching pulses for an LC-filtered VSI, all while using a minimal six-switch configuration.

PSD analysis confirms the method's effectiveness in evenly reducing acoustic noise and lowering THD to meet EMC standards. This leads to reduced motor vibrations, decreased heating in power converters and improved harmonic suppression, supporting smoother grid integration with renewable energy. Future research will focus on real-time experimental validation, adaptive recurrent neural implementations for dynamic load variation and exploration of multi-objective optimisation to balance EMI suppression with switching losses.

References

Addo-Yeboah, B. and Owusu, G. (2022). Modification of SPWM-based controller for voltage source inverter. *14th International Conference on Electronics, Computers and Artificial Intelligence (ECAI), IEEE*. Ploiesti, Romania, 30th June – 01st July 2022.

A. C. Binojkumar and G. Narayanan, "Variable switching frequency PWM technique for induction motor drive to spread acoustic noise spectrum with reduced current ripple," in *Proc. IEEE Int. Conf. Power Electronics, Drives and Energy Systems (PEDES)*, Mumbai, India, Dec. 2014, pp. 126–150, doi: 10.1109/PEDES.2014.7042071.

Ali, A. and Mashwani, W. K. (2023). A Supervised Machine Learning Algorithms: Applications, Challenges, and Recommendations. *Proceedings of the Pakistan Academy of Sciences: A Pakistan Academy of Sciences*, 60(4), pp. 1–12. doi: 10.53560/PPASB(60-sp1)editorial

Bech, M. M., Blaabjerg, F. and Pedersen, J. K. (2000). Random Modulation Techniques With Fixed Switching Frequency for Three-Phase Power Converters. *IEEE Transactions on Power Electronics*, 15(4), pp. 753–761. doi: 10.1109/63.849046

Bhattacharya, S., Mascarella, D., Joos, G. and Moschopoulos, G. (2015). A discrete random PWM technique for acoustic noise reduction in electric traction drives. *IEEE Energy Conversion Congress and Exposition (ECCE)*. Montreal, QC, Canada, 20-24 September 2015.

Boudjerda, N., Boudouda, A., Melit, M., Nekhoul, B., El Khamlichi Drissi, K. and Kerroum, K. (2011). Optimized dual randomized PWM technique for reducing conducted EMI in DC-AC converters. *IEEE International Symposium on Electromagnetic Compatibility*. York, UK, 26-30 September 2011.

Boudouda, A., Boudjerda, N., Melit, M., Nekhoul, B., El Khamlichi Drissi, K. and Kerroum, K. (2012). Optimized RPWM technique for a variable speed drive using induction motor. *International Symposium on Electromagnetic Compatibility - EMC EUROPE*. Rome, Italy, 17-21 September 2012.

de Oliveira, A., da Silva, E., Jacobina, C. B. and Lima, A. M. N. (2005). Random space vector modulation for 3-level power inverters and induction motor drives current control. *IEEE PESC*. pp. 987–993, Dresden, Germany, 16-16 June 2005.

Haq Syed Abdul, S., JeyaRohini, R., Meenalochini, P., Jeyakanth, K., Immanuvel, C. and HarishBabu, T. (2021). A Sinusoidal Pulse Width Modulation (SPWM) Technique for Capacitor Voltage Balancing of Nested I-Type Four-Level Inverter. *Materials Today: Proceedings*, 45(2), pp. 2435–2439. doi: 10.1016/j.matpr.2020.11.014

J. W. Makhubele and K. A. Ogudo, "Analysis of Harmonic Contents of Hysteresis-band Current Controller Pulse Width Modulation Technique on a Single-Phase Full-Bridge Inverter Using MATLAB Software," Cape Town, South Africa, 09-10 December 2021.

Jadeja, R., Ved, A. D. and Chauhan, S. K. (2015). An Investigation on the Performance of Random PWM Controlled Converters. *Engineering, Technology and Applied Science Research*, 5(6), pp. 876–884. doi: 10.48084/etasr.599

Kaboli, S., Mahdavi, J. and Agah, A. (2007). Application of Random PWM Technique for Reducing the Conducted Electromagnetic Emissions in Active Filters. *IEEE Transactions on Industrial Electronics*, 54(4), pp. 2333–2343. doi: 10.1109/TIE.2007.899944

Kazem, A. H. (2007). Input current waveshaping methods applied to single-phase rectifier. *International Conference on Electrical Machines and Systems* (ICEMS). Seoul, Korea, 08-11 October 2007.

Khan, H., Touzani, Y. and Drissi, K. E. K. (2010). Random space vector modulation for electric drives: A digital approach. *14th International Power Electronics and Motion Control Conference, EPE-PEMC*, Ohrid, Macedonia, 06-08 September 2010

Kim, J. G., Jung, Y. G., Na, S. H. and Lim, Y. C. (2004). A new random PWM (SRP-PWM) technique for decreasing acoustic noise radiated from v/f controlled motor drives. *30th Annual Conference of IEEE Industrial Electronics Society, IECON 2004*. Busan, Korea (South), 02-06 November 2004.

Kirlin, R. L., Lascu, C. and Trzynadlowski, A. M. (2011). Shaping the Noise Spectrum in Power Electronic Converters. *IEEE Transactions on Industrial Electronics*, 58(7), pp. 2780–2788. doi: 10.1109/TIE.2010.2076417

Kuebrich, K., Duerbaum, T., Stadler, A. and Schetters, K. (2005). Influence of nonlinear magnetic inductance in passive mains harmonic reduction circuits. *Twentieth Annual IEEE Applied Power Electronics Conference and Exposition, APEC*. Austin, TX, 6-10 March 2005.

Lai, Y., Chang, Y. and Chen, B. (2013). Novel Random-Switching PWM Technique With Constant Sampling Frequency and Constant Inductor Average Current for Digitally Controlled Converter. *IEEE Transactions on Industrial Electronics*, 60(8), pp. 3126–3135. doi: 10.1109/TIE.2012.2201436

Lee, C., Hui, S. and Chung, H. (2000). A Randomized Voltage Vector Switching Scheme for 3-Level Power Inverters. *PESC*, 1, pp. 27–32. doi: 10.1109/PESC.2000.878794

Lee, K., Shen, G., Yao, W. and Lu, Z. (2016). Performance characterization of random pulse width modulation algorithms in industrial and commercial adjustable speed drives. *IEEE Applied Power Electronics Conference and Exposition (APEC)*. Long Beach, CA, USA, 11-12 October 2016.

Liaw, C. M., Lin, Y. M., Wu, C. H. and Hwu, K. I. (2000). Analysis, Design, and Implementation of a Random Frequency PWM Inverter. *IEEE Transactions on Power Electronics*, 15(5), pp. 843–854. doi: 10.1109/63.867673

Madasamy, P., Verma, R., Bharatiraja, C., Barnabas Paul Glady, J., Srihari, T., Munda, J. L. and Mihet-Popa, L. (2021). Hybrid Multicarrier Random Space Vector PWM for the Mitigation of Acoustic Noise. *Electronics*, 10(12), pp. 1–19. doi: 10.3390/electronics10121483

Mahalik, F. and Kos, D. (2005). Conductive EMI reduction in DC-DC converters by using the randomized PWM. *Proceedings of the IEEE International Symposium on Industrial Electronics, ISIE*. Dubrovnik, Croatia, 20-23 June 2005.

Makhubele, J. W. and Ogudo, K. A. (2021). Analysis of harmonic contents of hysteresis-band current controller pulse width modulation technique on a single-phase full-bridge inverter using MATLAB Software. *International Conference on Electrical, Computer and Energy Technologies* (ICECET). Cape Town, South Africa, 09-10 December 2021.

Mathe, L., Lungeanu, F., Sera, D., Rasmussen, P. O. and Pedersen, J. K. (2012). Spread Spectrum Modulation by Using Asymmetric-Carrier Random PWM. *IEEE Transactions on Industrial Electronics*, 59(10), pp. 3710–3718. doi: 10.1109/TIE.2011.2179272

Mathews, M., Ramesh, B. and Sreedhar, T. (2022). Minimization of THD in Nine Level Cascaded H-Bridge Inverter Using Artificial Neural Network. *International Journal of Innovative Works in Engineering and Technology (IJIWET)*, 4(1), pp. 1–12. doi: 10.48550/arXiv.2205.13366

Muhlethaler, J., Schweizer, M., Blattmann, R., Kolar, J. W. and Ecklebe, A. (2013). Optimal Design of LCL Harmonic Filters for Three-Phase PFC Rectifiers. *IEEE Transactions on Power Electronics*, 28(7), pp. 3114–3125. doi: 10.1109/TPEL.2012.2225641

Muthukumar, P. and Mary, P. M. (2014). A co-simulation of random pulse width modulation generation. *IEEE, International Conference on Circuits, Power and Computing Technologies [ICCPCT-2014]*. Nagercoil, India, 20-21 March 2014.

Owusu, G., Annan, J. K. and Nunoo, S. (2023). Neural Network-Based Optimisation of Sinusoidal PWM

Controller for VSI-Driven BLDC Motor. *Power Electronics and Drives*, 8(43), pp. 275–298. doi: 10.2478/pead-2023-0018

Peyghambari, A., Dastfan, A. and Ahmadyfard, A. (2016). Selective Voltage Noise Cancellation in Three-Phase Inverter Using Random SVPWM. *IEEE Transactions on Power Electronics*, 31(6), pp. 4604–4610. doi: 10.1109/TPEL.2015.2473001

Raju, N. I., Islam, M. S. and Ahmed, A. U. (2013). Sinusoidal PWM Signal Generation Technique for Three Phase Voltage Source Inverter With Analog Circuit & Simulation of PWM Inverter for Standalone Load & Micro-Grid System. *International Journal of Renewable Energy Research*, 3(3), pp. 647–658. doi: https://doi.org/10.20508/ijrer.v3i3.771.g6188

S. D. George and M. R. Baiju, "Random pulse width modulation technique for a 4-level inverter," in *Proc. IEEE 7th Int. Power Engineering and Optimization Conf. (PEOCO)*, Langkawi, Malaysia, 2013, pp. 369–374, doi: 10.1109/PEOCO.2013.6564575.

Sohaib Sajid, H. M., Bilal Shafi, M., Malik, N., Muhammad, A. and Amin, A. (2020). Design of three phase inverter system with LC filter. *IEEE 23rd International Multitopic Conference (INMIC)*. Bahawalpur, Pakistan, 05-07 November 2020.

Wang, B., Drissi, K. E. K. and Fontaine, J. (2003). Modeling of the power spectrum density of an entirely randomized modulation in power converters. *IEEE International Symposium on Electromagnetic Compatibility, 2003. EMC '03*. Istanbul, Turkey, 11-16 May 2003.